PHYSICAL REVIEW B

CONDENSED MATTER

THIRD SERIES, VOLUME 48, NUMBER 10 1 SEPTEMBER 1993-II

Near-threshold ion-induced defect production in graphite

D. Marton, K. J. Boyd, T. Lytle, and J. W. Rabalais
Department of Chemistry, University of Houston, Houston, Texas 77204
(Received 1 March 1993)

Subplantation of the noble-gas ions He^+, Ne^+, Ar^+, and Kr^+ into graphite in the energy range of 10–150 eV with doses in the range of $1-15\times10^{14}$ ions/cm^2 has been studied by Auger electron spectroscopy (AES) and computer simulations. A technique based on AES line-shape analysis has been employed to describe quantitatively the ion-induced damage to the lattice. The carbon *KLL* AES line shapes and the AES spectra from subplanted Ne, Ar, and Kr were used to determine the ion penetration thresholds E_p, ion displacement thresholds $E_{\rm th}$, and the lattice displacement energies E_d. The E_p's scale linearly with the atomic radius of the projectiles. Defect production begins at E_p, although these energies are below $E_{\rm th}$. A mechanism for defect production at energies below $E_{\rm th}$ based on noble-gas interstitials and lattice strain and distortion is developed. This process is modeled through the CHARMM molecular modeling program and the TRIM classical trajectory simulation.

I. INTRODUCTION

The energy thresholds for penetration and defect formation by low-energy ions impinging on surfaces is of great importance for film deposition technologies such as ion-beam deposition (IBD), ion-beam-assisted deposition, and plasma deposition. In these technologies, low-energy ions arrive at the surface of the substrate in the initial deposition stage and at the surface of the film itself at later stages of deposition. These ions may be incorporated into the solid where they may create strain and collisional defects. These processes are generally not well understood. Information available on the energy thresholds at which such processes begin to occur is limited. Interstitials due to insertion of the deposited species into an existing matrix are probably the most common point defects created at low deposition energies.

The critical low-energy values can be defined as follows. The minimum ion kinetic energy required for the projectile ion (i) to penetrate below the first atomic layer of the surface is the *penetration threshold* E_p and (ii) to cause displacements of lattice atoms is the *displacement threshold* $E_{\rm th}$. The kinetic energy acquired by a lattice atom as a result of a collision must be above a minimum *displacement energy* E_d for the lattice atom to be permanently displaced from its equilibrium site while leaving a vacancy. Because of mass mismatch of the projectile and lattice atoms, $E_{\rm th} > E_d$.

Displacement energies E_d have been studied using high-energy electron collisions for the last 40 years; such data pertain to bulk displacements. A recent paper gives an extensive table on such experimental E_d data available for various elemental and compound solids.[1] However, there is very little data available for surface E_d's, even though they could differ from those of the bulk. Also, there is virtually no data measured from ion impact, although E_d may vary depending on the mass and chemical characteristics of the projectiles. For example, a heavy projectile may remain in the vicinity of the Frenkel pair it created, thereby influencing the recombination probability. Also, the projectile may lose energy through inelastic electronic interactions. In fact, the present study was stimulated by such questions, i.e., whether or not E_d's due to ions reveal such tendencies. The importance of the E_d's for IBD processes has been recognized in particular for the case of the deposition of dense tetrahedral carbon films in the subplantation model,[2] which today is considered to be the most likely explanation for the formation of such films.

Measurements[3–5] of penetration thresholds E_p for different noble-gas ions on the same metal surface (W{100}) show that E_p increases with increasing atomic radii of the projectile and that it is sensitive to the surface orientation. The significance of E_p in the mechanism of film growth has been discussed in an early paper by Carter and Armour.[6] It is clear that the ion kinetic energy may play two slightly different roles in IBD. (1) It increases the mobility of the atoms at or near the surface,

 ©1993 The American Physical Society

thereby enabling them to overcome energetic barriers and form metastable compounds and/or structures. (2) It propels the impinging ion beyond the surface layer and allows nucleation and growth to occur in subsurface layers, i.e., subplantation.[2] This latter process may be responsible for the high density of IBD carbon films and for the excellent adhesion of IBD films in general. However, process (2) will only occur if the ions have kinetic energies above E_p. Consequently, if the processes responsible for the quality of a certain IBD film are related to process (1) only, then kinetic energies below E_p may be used successfully. In fact, the use of such lower energies may be advantageous in order to minimize defects. The minimum useful energy in this case will be determined by the energy barriers which have to be overcome. Such barrier energies are probably in the eV range. If process (2) plays an important role, however, then kinetic energies above E_p are necessary; these thresholds can be several tens of eV or higher.

The purpose of this paper is to determine the E_p, $E_{\rm th}$, and E_d values and the defect production rates R for the noble-gas ions He^+, Ne^+, Ar^+, and Kr^+ impinging on a graphite surface. In a previous paper, we have shown that carbon *KLL* Auger line-shape analysis can be used to measure defect production near the graphite surface resulting from low-energy ion impact.[7] The defect density can be quantitatively assessed by introducing a shape factor which describes the Auger line-shape changes observed a few eV below the Fermi level. This method was used to determine E_d and R as a function of ion kinetic energy for low-energy Ne^+.[8] In this paper we will briefly describe this method of E_d measurement. Auger measurements of (i) the carbon *KLL* line shapes resulting from irradiation by the four noble-gas ions as a function of ion energy and dose and (ii) the noble gases Ne, Ar, and Kr subplanted in graphite will be presented. Some of the Kr Auger data have been reported elsewhere.[9] On the basis of these data, we find E_p's which scale linearly with the atomic radii of the rare-gas atoms; only for ion energies above these E_p's can Auger signals from the subplanted noble-gas atoms be observed. The $E_{\rm th}$'s, E_d's, and R's are determined from this data. Defect production is observed for all energies above E_p, even at energies below E_d. A possible mechanism for defect production at energies below the E_d which involves noble-gas interstitials and lattice distortion of graphite in the surrounding area has been explored using the molecular modeling code CHARMM.[10] Results of these calculations show increasing distortion of the graphite lattice with the increasing atomic radius of the inserted atom.

II. EXPERIMENTAL METHODS

Highly oriented pyrolithic graphite samples (Union Carbide Co.) were irradiated by low-energy, mass-selected ion beams with current densities of ≈ 1 μA/cm^2 as described elsewhere.[7] Auger-electron-spectra (AES) of these irradiated samples were measured with a Perkin-Elmer double-pass cylindrical mirror analyzer (CMA) in the pulse-counting mode using 3 keV electron excitation at a current density of ≈ 1 mA/cm^2. The ion doses were measured as time integrals of the ion current continuously monitored on the sample. Only graphite samples with visibly perfect shiny surfaces were used. The pressure in the deposition chamber during the AES measurements was typically $<2\times10^{-9}$ Torr. No oxygen or other contaminants were detected by AES on the initial and/or damaged graphite surfaces. Further details of the experiments are similar to those described previously.[7-9]

Each experimental sequence was started by measuring the AES spectra of undamaged graphite in the 20–60 and 240–300-eV regions. Next, a rare-gas-ion dose of about $D=1\times10^{14}$ ions/cm^2 with a given kinetic energy was delivered to the sample and AES measurements were made on both the graphite energy regions and the regions expected for rare-gas signals. For each ion-irradiation dose and for each AES measurement, the sample was rotated into a position perpendicular to the ion beam and the CMA axis, respectively. The ion doses were increased until significant changes in the carbon *KLL* spectra were observed, but not exceeding $D=3\times10^{15}$ ions/cm^2. Typically, five- to eight-dose steps were used at each ion energy. The AES intensity ratios (rare gas/carbon) were used to determine the E_p's, with the exception of He, which is discussed in Sec. V B. Changes in the carbon *KLL* line shapes were used to monitor the defect production rate as described in Sec. III C.

III. EXPERIMENTAL RESULTS

A. Subplantation of noble gases into graphite

Neon, argon, and krypton trapped in graphite can be detected by AES, providing a simple and effective method for measuring the penetration thresholds E_p for these rare gases in graphite. Since adsorption of these gases is negligible at room temperature, any AES signal must come from atoms which have penetrated into subsurface layers of graphite and remain trapped. Figure 1 shows changes in the AES intensity ratios Ne(*KLL*)/C, Ar(*LMM*)/C, and Kr(*MNN*)/C as a function of ion dose. In each case, a dramatic change in the noble-gas AES yield is observed at a well-defined energy threshold. Below this penetration threshold, i.e., at 30 eV for Ne, 42 eV for Ar, and 45 eV for Kr, no noble gases were detected in graphite. An additional kinetic energy of just a few eV above these thresholds is sufficient for these gases to penetrate the surface and accumulate in amounts which are easily detected. It is very difficult to quantify the amounts of trapped noble gases, but it is estimated that they do not exceed a few atomic percent.

Figure 2 shows AES intensity ratios for Ar/C and Kr/C versus ion dose for various ion energies above the penetration thresholds. Interestingly, the amounts of these noble gases trapped in the graphite do not necessarily increase either with the kinetic energy or with the dose of the ions. It appears that the impinging ions may be removing some of the noble-gas atoms already trapped in the graphite.

B. Direct evidence for defect production

Direct evidence for defect production in graphite can be obtained from AES using the electron-diffraction effects observed at low electron energies, although this is neither a well-established nor well-understood area. Three AES integral spectra, i.e., $EN(E)$, in the 20–120 eV energy range are shown in Fig. 3. Since the large inelastic background at low kinetic energies makes it difficult to obtain reliable spectra in this region, these spectra were obtained by using 40 times the primary-electron dose usually applied in order to improve the statistics. A nine-point smoothing and fourth-order polynomial background subtraction were used to enhance the signal-to-background ratio. This treatment is not very reliable for the assessment of the peak intensities; therefore, such information is not utilized. Spectrum *a* was obtained on undamaged graphite with the CMA axis normal to the surface plane. The peaks at 26, 35, 44, 55, 66, 76, and 96 eV are characteristic for the undamaged graphite surface; their intensities are extremely sensitive to the alignment of the sample with respect to the CMA axis. Spectra *b* and *c* were obtained after Kr^+-ion bombardment.

The structure in the spectrum shown as curve *a* in Fig. 3 is related to interference processes from the graphite surface[11] and Coster-Kronig transitions in the graphite valence band.[12] When monoenergetic electrons are emitted from a symmetrical lattice structure, they give rise to an interference pattern which results in spatial anisotropy of the ejected electrons. Detection of these electrons with spatial resolution allows detection and recognition of surface symmetry, as is common in low-energy electron-diffraction (LEED) studies. In the case of a CMA with

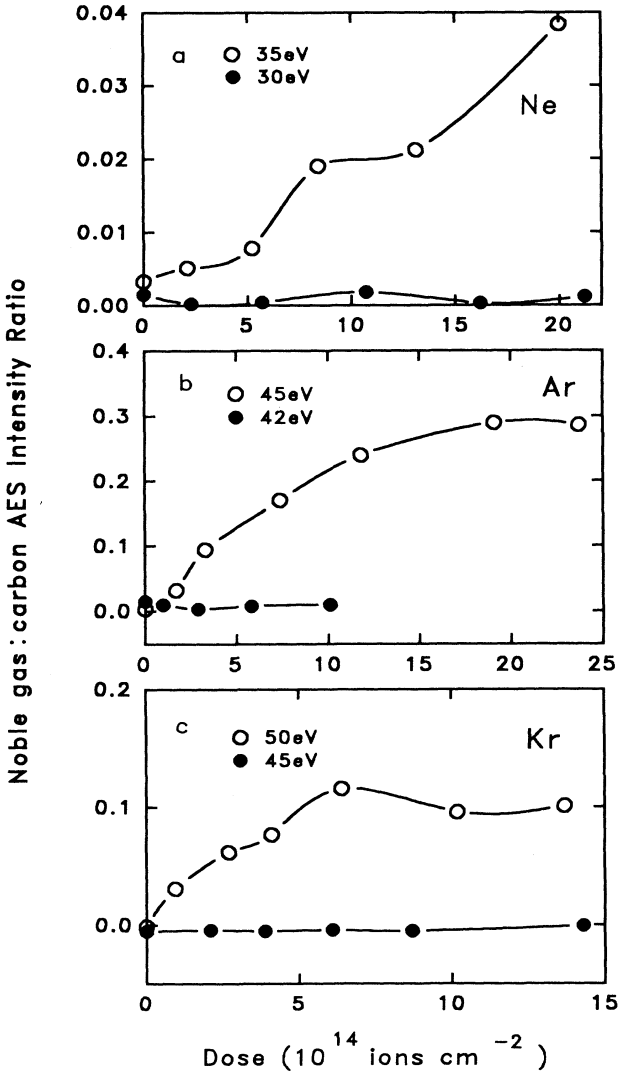

FIG. 1. AES intensity ratios below and above the penetration threshold. (a) Ne(*KLL*)/C(*KLL*), $E_p \approx 32.5$ eV; (b) Ar(*LMM*)/C(*KLL*), $E_p \approx 43.5$ eV (c) Kr(*MNN*)/C(*KLL*), $E_p \approx 47.5$ eV. The lines through the data points are drawn to guide the eye.

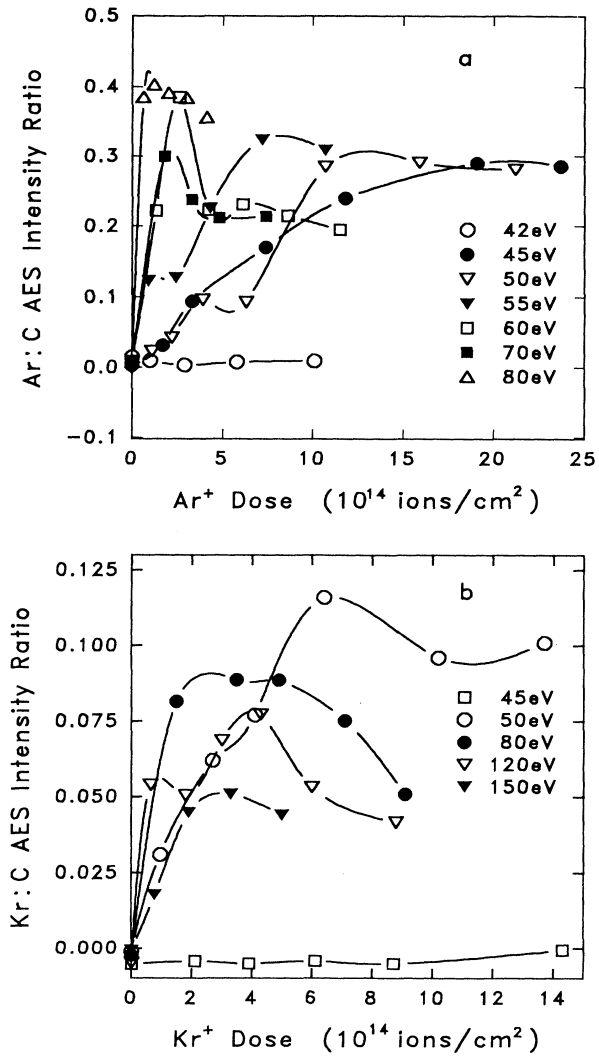

FIG. 2. AES intensity ratios vs Ar^+- and Kr^+-ion bombardment dose in graphite. (a) Ar(*LMM*)/C(*KLL*) and (b) Kr(*MNN*)/C(*KLL*). The lines through the data points are drawn to guide the eye.

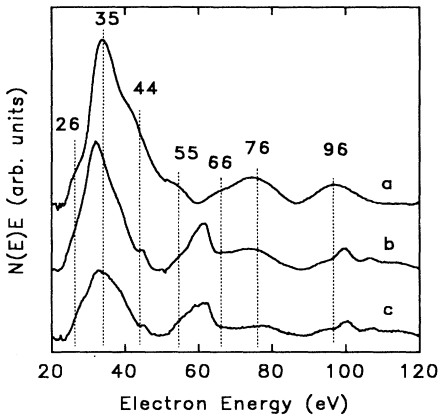

FIG. 3. Low-energy AES spectra from (a) undamaged and (b), (c) Kr^+-irradiated graphite. Note the Kr *MNN* peaks near 44 and 60 eV and the Coster-Kronig peak at 99 eV. (b) 1.0×10^{15} ions cm^{-2} at 65 eV and (c) 2.5×10^{14} ions cm^{-2} at 100 eV.

its axis perpendicular to the surface, only electrons leaving the surface near a single exit angle $\approx 42.3°$ are detected. Such a restriction leads to interference patterns which are observed as increased or decreased intensities at specific energies related to the surface symmetry. Any deviation from the perpendicular geometry results in broadening of the acceptance exit angle, which in turn broadens the energy dependence. The observation of these peaks at the perpendicular geometry provides a sensitive tool for directly monitoring the existence and destruction of the surface symmetry. One can calculate diffraction peak energies for graphite in the geometry used in our experiments. Diffraction peaks at 26, 68, 74, 76, 78, and 94 eV energies are predicted, in general agreement with the experiment except for the large peak at 35 eV. We believe that this peak results from a carbon VV^*V^* Coster-Kronig transition involving a doubly excited carbon atom. Such a transition can yield an electron with kinetic energy $E = E_m - 2E_n$, where E_m and E_n are the binding energies corresponding to the maxima of the bonding and antibonding σ densities of states, respectively. Since $E_m \approx 13$ eV and $E_n \approx -10$ eV,[13] an AES energy of ≈ 33 eV is highly probable.

The spectra shown as curves *b* and *c* in Fig. 3 indicate that Kr irradiation of the graphite surface destroys much of the structure observed in the spectrum shown as curve *a*; peaks due to subplanted Kr are also observed near 45, 62, and 99 eV. The 99-eV peak has been identified[9] as a Coster-Kronig transition which has only been observed in the spectra of solid Kr.[14] Although the interpretation of the peaks in the 20–120-eV region may not be fully understood, the AES spectra can be used as "fingerprints" to qualitatively follow the changes in the graphite structure. For this purpose, spectra obtained with much lower electron dose than those shown in Fig. 3 will suffice if the smoothing is followed by differentiation. Figure 4 shows a series of such spectra in the 20–80-eV region, which includes the Kr *MNN* line. These spectra clearly show the gradual disappearance of the graphite structure and the increase in embedded Kr in the graphite. The repeatability of the AES spectra in this low-energy region is relatively poor because it is very sensitive to the precise alignment of the sample and the focus of the CMA. These spectra were therefore evaluated only qualitatively, although the observed changes are quite dramatic.

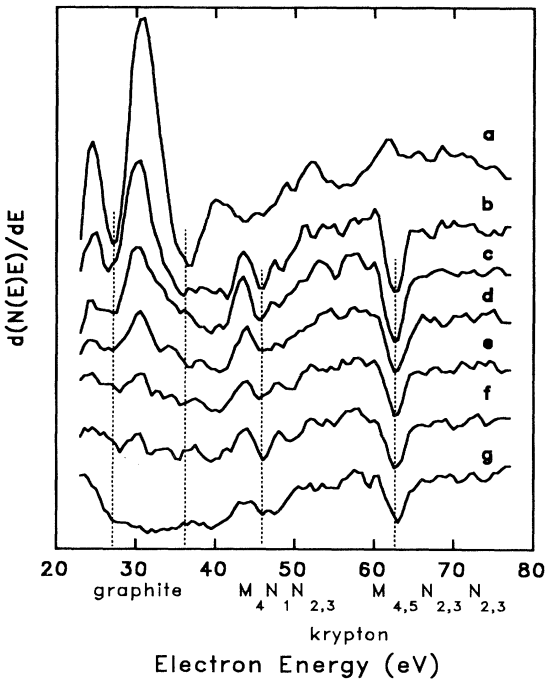

FIG. 4. Derivative AES spectra from (a) undamaged graphite and (b)–(g) 100-eV Kr^+-irradiated graphite. The doses are (b) 1.0×10^{14} cm^{-2}; (c) 1.8×10^{14} cm^{-2}, (d) 3.4×10^{14} cm^{-2}, (e) 5.3×10^{14} cm^{-2}, (f) 8×10^{14} cm^{-2}, and (g) 1.2×10^{15} cm^{-2}.

C. Defect-production-rate measurements

As we have shown previously for the cases of Ne^+- and C^+-ion impact on graphite, ion-beam damage to the graphite lattice leads to the development of a shoulder at about 280 eV in the $d(NE)/dE$ carbon *KLL* spectrum.[7] An example of a C *KLL* spectrum revealing such a shoulder as a result of Kr^+ irradiation is shown in Fig. 5. Such spectra were obtained after a nine-point smoothing and five-point differentiation. Although these changes in the carbon *KLL* spectra are small, they are fairly well understood and quite reproducible. The shoulder at 280 eV in the carbon AES line is a result of changes in the π density of states due to development of disorder in the graphite lattice. Such disorder disturbs the optimal p_z-p_z orbital overlap and gives rise to a reduction of the pseudo-band-gap between the π and π^* states. In the case of point defects, nonbonding *s* and *p* orbitals can give rise to a similar effective increase in the density of states in this energy region. This feature reveals the ion-impact-induced damage to the graphite surface, but does not distinguish between displacement defects and lattice strain due to embedded noble-gas atoms.

In order to quantify the shoulder at 280 eV, we introduced[7] a shape factor ratio $s = I/I_0$, where I and I_0 are

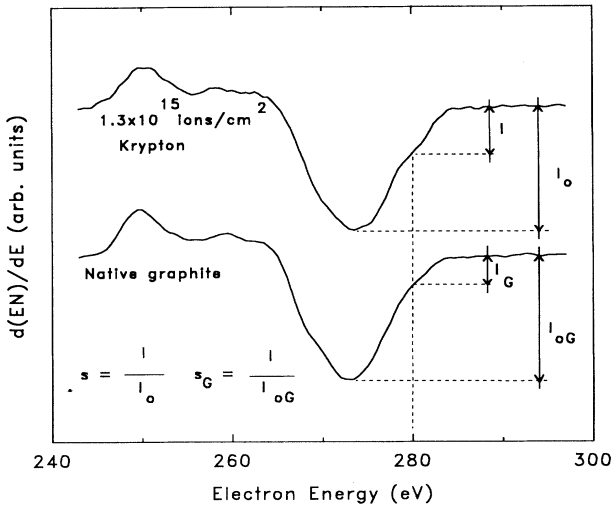

FIG. 5. Carbon *KLL* AES spectra of undamaged graphite and graphite after a dose of 1.3×10^{15} Kr^+/cm^2 at 100 eV. The shape-factor ratios are calculated from the intensities shown in the figure.

the AES intensities at the position of the 280-eV shoulder and at the minimum of the derivative, respectively, as illustrated in Fig. 5. According to our definition,

$$S=(s-s_G)/s_G \ . \tag{1}$$

Here s_G and s refer to undamaged and damaged graphite, respectively. The magnitude of the shape factor increases with ion dose if the ion energy is sufficiently high. This increase begins as a linear process as shown in Fig. 6 and saturates as damage to the surface becomes extensive.[7] At low doses when few defects are created, the initial defect production rate is expected to be independent of dose; hence, the number of defects should be linear with respect to dose. Since we observe a linear dose dependence for the shape factor, which is a measure of the defect density, the slope of the shape-factor increase with ion dose describes the defect production rate R.[8] These slopes are plotted as a function of ion energy for He^+, Ne^+, Ar^+, and Kr^+ in Fig. 7. The slopes were calculated as least-squares linear fits to the initial regions of shape-factor versus ion-dose curves, including the $S=0$ and dose$=0$ points. Thus the R values in Fig. 7 correspond to the defect production rate at each energy in the low-dose or initial-damage limit. Well defined thresholds are observed in all cases.

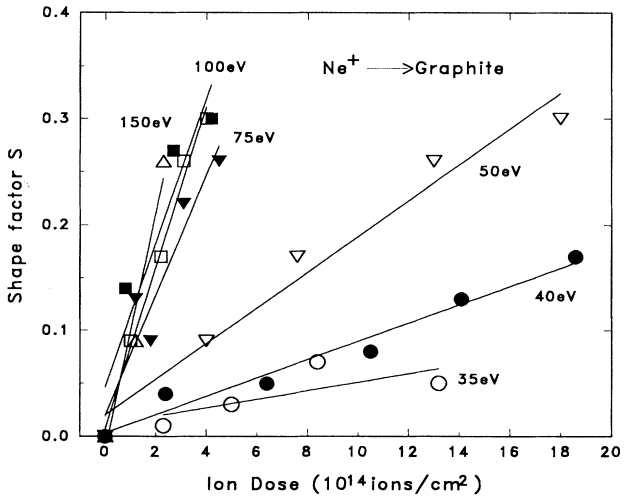

FIG. 6. Shape factors vs Ne^+-ion dose at various energies. The lines are linear least-squares fits to the data.

IV. MOLECULAR MODELING CALCULATIONS

The molecular modeling program CHARMM (Ref. 10) was used to model the noble gases in the graphite lattice. This program was developed in order to find equilibrium configurations of large molecules when the binding properties of the constituent atoms are known. We assumed for these calculations that the sp^2 character of the graphite bonds does not change due to the rare-gas interstitials and that these interstitials are not bound strongly to either the carbon atoms or to each other. The program uses empirical energy functions to model the macromolecular systems, and the energy is minimized with respect to the structural parameters. We used the CHARMM force field as implemented in QUANTA version 3.2.[15]

Graphite was modeled by five sheets of aromatic hexagonal carbon networks, each sheet staggered with respect to its neighbors at the onset of the calculation. The sheets were composed of 300 carbon atoms each, with hydrogen atoms added at the edges to terminate the dangling bonds. One of the peripheral layers represented the surface and the noble-gas atoms were positioned between this layer and the penultimate layer. When more than one noble-gas atom was used in the same calculations, e.g., two, three, or four neon atoms, these atoms were initially separated by at least 10 Å. In the process

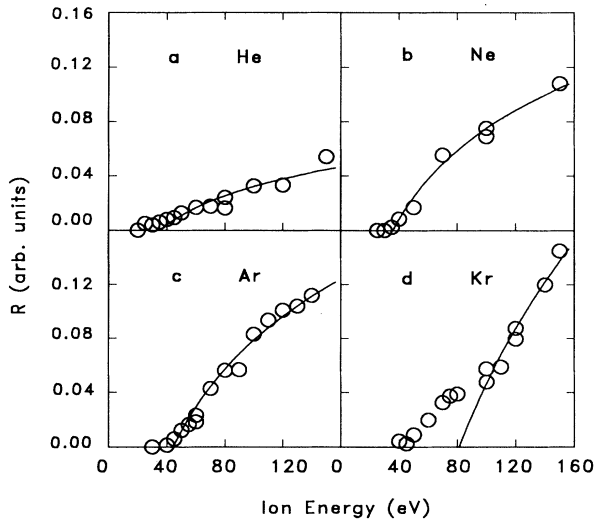

FIG. 7. Defect production rates R vs ion energy for (a) He^+, (b) Ne^+, (c) Ar^+, and (d) Kr^+ ions. The lines are logarithmic fits to the data as described in the text.

of energy minimization, the noble-gas atoms move to energetically more favorable positions and the graphite sheets become deformed with noticeable bulges in the top layer. If the calculation is allowed to go on for a very extended period of time, the noble-gas atom may find a way to migrate out from between the graphite layers while the graphite returns to its undeformed state. This is a trivial solution of the energy-minimum problem. In order to avoid this outcome, the calculations had to be terminated after having reached a nearly stationary state in which the noble-gas atoms move slightly around inside the graphite model with practically no change in the energy and/or shape of the system. The results reported here relate to such stationary states achieved typically after 125–175 iteration steps.

Figure 8 shows CHARMM calculation results for the case of one, two, and three Kr atoms. The first layer exhibits the greatest amount of distortion, with maximum out-of-plane bending along the c axis of ≈ 1.1 Å. When two or three Kr atoms are inserted, the energy minima are obtained when there is a single broad deformation under which the Kr atoms are forced together in order to minimize the layer buckling. The tremendous force required to move hundreds of graphite carbon atoms out of plane compresses the noble-gas atoms. Since these atoms cannot diffuse through the carbon layers, they assume close-packed arrays in order to minimize the C layer distortion.

The data obtained from similar calculations for the noble gases from He to Xe is summarized in Fig. 9 as a plot of first-layer bulge height versus the atomic radius of the noble gas (van der Waals radii, according to Ref. 16). From the linear fit, it appears that no deformation would occur if the noble-gas radius were less than 99 pm. The largest interstitial space between the layers of the graphite lattice has a radius of 120 pm, suggesting that a species of lesser atomic radius would not cause deformation. The actual limit may, however, be at a smaller atom size because of the fact that the atom sizes depend on the surrounding environment. It is known that in intercalated graphite compounds the graphite sheets become aligned,[17] providing a larger interstitial site. Since the CHARM program does not allow for such sheet alignments, our calculations relate to results for staggered graphite sheets. It is possible that the shift of the carbon sheets in intercalated compounds is related to electronic and not merely steric effects or that more than just a few percent of a monolayer rare-gas concentration would be necessary to trigger the alignment. In either case, such an effect may not be expected in the case of noble-gas interstitials in our experiments.

It is remarkable that the deformation forces of the graphite sheets result in close packing of the noble-gas atoms. This process is limited by the repulsive forces between the noble-gas atoms. It results in an equilateral triangular arrangement in the case of three noble-gas atoms and a rhomboidal arrangement in the case of four noble-gas atoms. For a given noble gas, the interatomic distances between the noble-gas atoms are the same for the case of two, three, or four atoms and these distances are

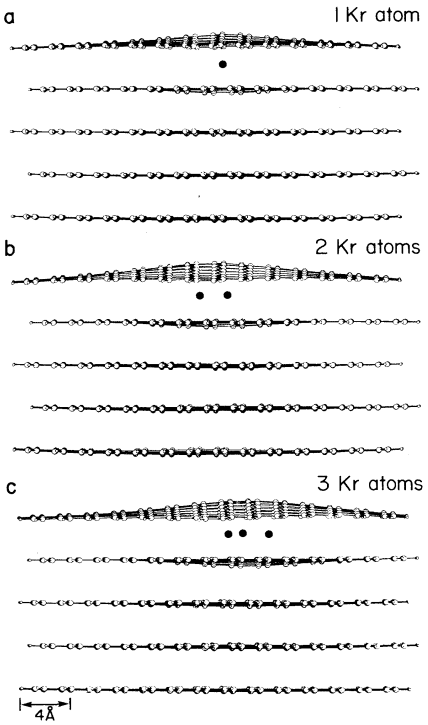

FIG. 8. Molecular modeling simulation for Kr atoms subplanted between the first two layers of graphite. The solid circles represent the noble-gas atoms. The distances between the atoms is subject to distortion due to the planar representation. Note the large distortion of the first carbon layer in the form of a bulge due to the subplanted atoms.

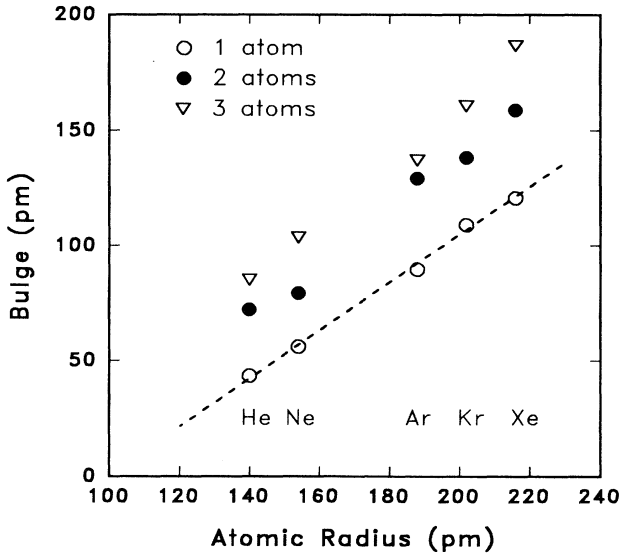

FIG. 9. Distortion bulge heights of the first graphite layer from calculations similar to those illustrated by Fig. 8 due to the presence of various noble-gas atoms between the outermost layers. The dotted line is a linear least-squares fit to the single-atom data. The zero bulge intercept at 99 pm indicates the noble-gas atom size that would not cause a bulge.

less than the interatomic distances in the crystalline forms of the gases. For example, the nearest-neighbor distance in a krypton crystal is 385 pm, but in graphite the calculated Kr-Kr distance is only 276 pm.

V. DISCUSSION

A. Penetration thresholds E_p

Measurements described in Secs. III A and III B show that the same thresholds which were observed for the penetration of each noble-gas species into graphite appear also to be thresholds for defect production. The same conclusion is evident from the comparison of Figs. 1(a) and 6; this conclusion holds for both Ar and Kr as well. We will show later that these E_p's are at lower energies than the E_{th}'s; hence, defect production by processes other than displacement must be considered. Such processes can be lattice distortions due to penetration and trapping of noble-gas atoms in the lattice.

The penetration thresholds E_p found in this work are summarized in Fig. 10 as a plot of E_p versus the atomic radius of the noble-gas ion. Data based on AES evidence for noble-gas penetration into the graphite, such as shown in Fig. 1, are used for the cases of Ne, Ar, and Kr. These penetration thresholds in all these cases coincide with the onset of defect production in graphite as data based on carbon line-shape analysis show (c.f. Fig. 7). In the case of He, the subplanted gas cannot be detected directly by AES, but the carbon-defect production data are available, providing a penetration threshold of 20–25 eV. This conclusion is based both on data in the 20–60 eV region similar to those shown in Fig. 3 and on carbon KLL line-shape changes. The least-squares straight line through the penetration threshold data in Fig. 10 allows one to determine an extrapolated value of 75 pm for the atomic radius of an atom for which $E_p=0$; i.e., no energy is expended for such an atom to penetrate the graphite lattice. Hence a projectile with an atomic radius <75 pm can penetrate the graphite lattice with no extra energy, provided that the interaction between this projectile and the carbon lattice is negligible. In the present work, we were unable to check the validity of this conclusion, but it appears to be quite reasonable. The carbon atoms in the graphite lattice form hexagonal rings with hollow centers of radius 77 pm; i.e., the size of a carbon atom. Ions with lesser radii should be able to travel through such rings without impediment.

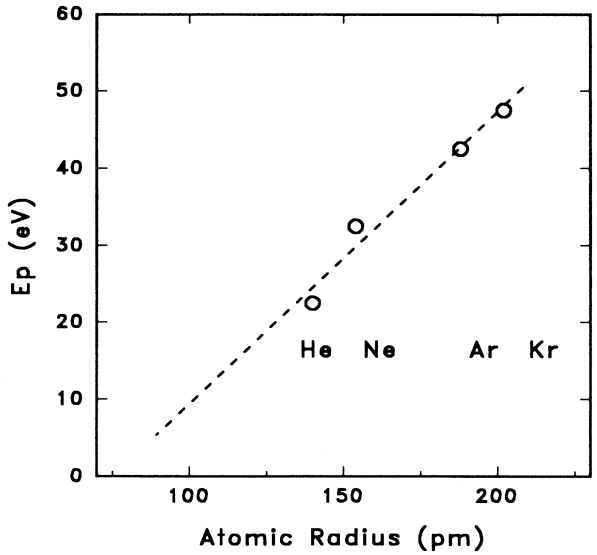

FIG. 10. Penetration thresholds of rare gases in graphite as a function of the atomic radius of the rare gas. The dotted line is a linear least-squares fit to the data. The zero intercept at 75 pm indicates that an inert atom of this size could penetrate into graphite without expenditure of kinetic energy.

B. Displacement thresholds E_{th} and displacement energies E_d

Comparison of Figs. 2 and 6 shows that the processes revealed by these two types of measurements are quite different. In Fig. 2 we observe rare-gas penetration and capture as a process which quickly saturates with both ion dose and kinetic energy. In Fig. 6 we observe a process which intensifies with both ion dose and kinetic energy. This latter process is production of displacement defects. In order to elucidate this phenomenon, we use the summary of data presented in Fig. 7.

The energy dependence of the defect-production-rate R data for different noble-gas ions (Fig. 7) reveals some significant differences in the collisions of these ions. It appears that the overall R in the case of He is less than that of the other noble gases investigated. We have carried out TRIM calculations[18] in order to clarify this situation; the results are shown in Fig. 11. The main difference between He and the other noble gases is that He penetrates significantly deeper into carbon. Thus, even though the number of total displacements is similar [cf. Fig. 11(a)]; the number of displacements, and perhaps any other defects, in the top 10 Å is different [cf. Fig. 11(b)]. Since we use AES to detect the defects and since AES is very surface sensitive (for carbon *KLL* electrons the attenuation length is ≈ 5.5 Å), this difference in the projected ranges results in a lower sensitivity of our measurement for He compared to the other noble gases. This, in turn, results in less reliability of the He data than the other data in Fig. 7.

In evaluating the defect production data of Fig. 7, we followed standard procedures which have been well established for the case of electron-impact displacement energy measurements. We have previously described these procedures[8] and will repeat them here only briefly. The defect production rate R can be related to the probability of collisional defect production P, the projectile kinetic energy T, and the collisional cross section σ by the expression[19]

$$R=\int_{E_d}^{T} P(T)\frac{d\sigma}{dT}dT \ . \tag{2}$$

This expression is based on the assumptions that defects are detected in numbers proportional to the defect production rate and that they are independent of time elapsed since the defects were created and T has been expended. In order to evaluate expression (2), one has to

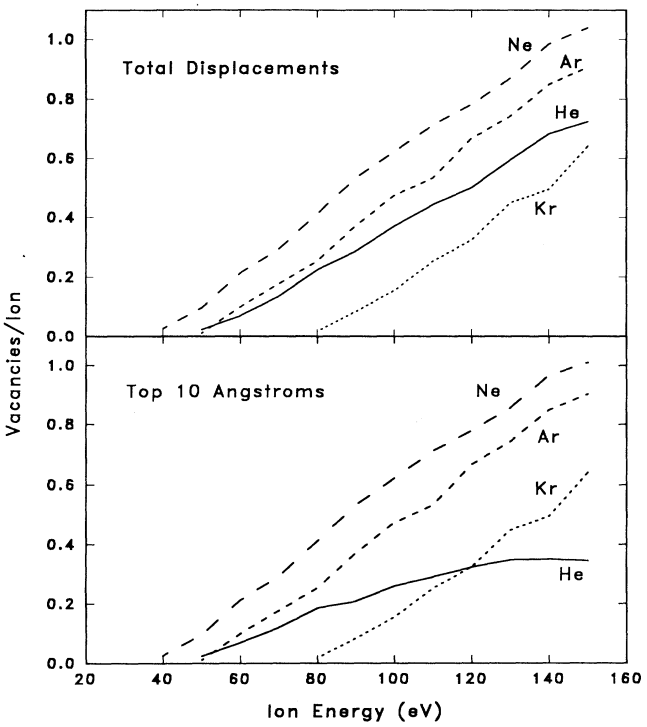

FIG. 11. Total displacements or vacancies created in graphite by noble-gas ions of various energies as calculated by TRIM89. Full cascades were generated and 33 eV was used as the input displacement energy of graphite.

set up a model for the processes including the collisional cross section and defect production probability. The collisional cross sections are not well known in the very-low-kinetic-energy range. We employed the Lindhard power potential in order to retain the advantages of an analytical solution.[20] According to this approach,

$$d\sigma(T)\sim E^{-m}T^{-m-1}dT\ , \tag{3}$$

where $m\approx 0.2$ yields a relatively good fit to the Biersack-Ziegler universal potential.[21] Calculations were carried out with $m=0.2$ and 0. The latter value leads to a simple logarithmic curve for R, provided that the probability is a step function. Since the scatter of our data does not permit us to distinguish between these two choices of m, the simpler solution with $m=0$ was used.

The defect creation probability, according to the usually used assumptions, is either a simple step function ($P=0$ below threshold and $P=1$ above threshold) or a linear transition region (P varies from 0 to 1 over a finite region centered at the threshold).[22] Again, since the precision of our data is insufficient to distinguish between these possibilities, we adopted the simpler approach. Logarithmic fits are relatively easily made to the Ne and Ar data [Figs. 7(b) and 7(c)]. These fits yield $E_{\rm th}=37.0$ eV for neon and $E_{\rm th}=47.3$ eV for argon with $r=0.9902$ and 0.9913, respectively. Because of the mass difference between the projectile M_1 and the target M_2, the energy-transfer factor γ and the displacement energy can be described by

$$\gamma=(4M_1M_2)/(M_1+M_2)^2 \tag{4}$$

and

$$E_d=\gamma E_{\rm th}\ . \tag{5}$$

The atomic radii, penetration and displacement thresholds, energy-transfer factors, and displacement energies are summarized in Table I. Apparently, the differences in $E_{\rm th}$ for Ne and Ar are compensated by the energy-transfer factors to yield E_d's which are only about 1 eV apart. Also, in the case of Ne and Ar, the E_p's are only slightly lower than the $E_{\rm th}$'s. If one would assume that the same is true for the case of Kr, then E_d in that case would appear to be much lower than in the case of Ne and Ar. Moreover, the logarithmic fit to the Kr rate data of Fig. 7 would be quite poor. Considering the noticable discontinuity in the Kr rate data of Fig. 7 near 80 eV, it appears to be a better assumption that in this case $E_{\rm th}$ is significantly above E_p due to the very low energy-transfer efficiency γ. With this assumption, the data for $E<80$ eV were excluded from the fitting procedure in the Kr case. This leads to a satisfactory logarithmic fit (regression coefficient $r=0.9832$) and an E_d value which is close to the values obtained for Ne and Ar. According to this interpretation, the defect production for $E<80$ eV is due to a process other than direct displacement, such as the lattice distortion described in Sec. IV.

The He rate data (Fig. 7) are of relatively poor quality because of the small amount of damage. The onset of measurable defect production is in the 20–25-eV range. If one had only this information, a logarithmic fit to these data would yield a very low $E_{\rm th}$ and E_d, although it is an extremely poor fit to the data. We are unaware of any physical process for the He case which would lead to such an exceptionally low E_d value. We can, however, assume an approach similar to that of Kr and use only the results at higher energies. On this basis we obtain a reasonable fit ($r=0.9248$) along with $E_{\rm th}$ and E_d values in broad agreement (Table I) with the other noble gases.

TABLE I. Summary of the penetration thresholds E_p, displacement thresholds $E_{\rm th}$, and displacement energies E_d determined herein along with atomic radii and mass-transfer factors γ.

Rare gas	Atomic radius (Å)	E_p (eV)	$E_{\rm th}$ (eV)	γ (eV)	E_d (eV)
He	1.40	22.5±2.5	40.0	0.75	30.0±1
Ne	1.54	32.5±2.5	37.0	0.94	34.7±1
Ar	1.88	43.5±1.5	47.3	0.71	33.6±1
Kr	2.02	47.5±2.5	80.8	0.44	35.3±1

We emphasize that the precision of the He data is insufficient for drawing further conclusions. The merit of this evaluation is that it shows that all of our data can be consistent with a single model for defect production due to penetration at lower energies and displacement above a unique threshold.

Earlier displacement energy studies on graphite found $E_d \approx 33$ eV (Refs. 23 and 24) and no differences in the surface and bulk[24] E_d's. Our average value of E_d(ave) $\approx$ 34.5 eV is slightly higher, although the addition of more data herein has resulted in a lower figure for Ne compared to our previously published value of $E_d = 35.3$ eV. We found no clear trend for a mass dependence in the E_d values.

The changes in the carbon KVV spectra are due to shifts in the π energy levels and density of states in graphite. This effect can be caused by point defects or by buckling as predicted by the molecular modeling calculations. However, it is not excluded that a similar effect might arise from other processes, such as the alignment of the carbon planes, while preserving planarity as in intercalation. There is, however, direct evidence for the existence of the clustering effect predicted by the molecular modeling. We found distinct similarities between our Kr MNN spectra from the gas embedded in graphite and spectra observed from solid krypton[14,25] at low temperature. The minima at 46 and 63 eV in Fig. 2 and the Coster-Kronig transition at ~ 100 eV are all characteristic of solid Kr. Since the Kr-Kr attraction energy is $\ll kT$ at room temperature, this clustering must be a result of the forces exerted by the carbon lattice. The simplest explanation for this is the buckling predicted by the CHARMM calculations.

VI. SUMMARY

Direct irradiation of graphite surfaces with low-energy noble-gas ions coupled with AES line-shape analysis has been used to probe penetration and defect production thresholds and defect production rates for low ion doses. The most significant results can be summarized as follows.

(i) The minimum energy E_p required for the noble-gas ions to penetrate below the graphite surface can be detected by AES. The measured E_p's increase linearly with ion radius from 22.5±2.5 eV for He to 47.5±2.5 eV for Kr. The E_p for He is measured as the onset of ion damage, which in all other cases coincides with E_p.

(ii) Direct evidence for ion damage can be obtained from analysis of the low-energy (20–60 eV) AES spectra, where symmetry-related peaks appear from the undamaged graphite.

(iii) Detailed analysis of the carbon KVV transition allows quantitative analysis of the defects and the defect production rate. The experimental data were found to be consistent with a displacement energy value of $E_d = 34.5 \pm 1$ eV, which is independent of mass for Ne, Ar, and Kr. The He data are not sufficiently reliable for quantitative comparison. The defect production rates exhibit a logarithmic increase with increasing ion energy, with some notable deviations in the low-energy region.

(iv) These results indicate that defects are produced at ion energies that are sufficient for penetration, i.e., E_p, but insufficient for causing collisional damage in the form of atomic displacements, i.e., below E_d. A plausible mechanism for such defect formation is the strain of the lattice resulting from interstitial rare-gas atoms.

(v) The mechanism of lattice strain was explored through CHARMM molecular modeling calculations. These calculations indicate an increasing distortion, in the form of a bulge in the carbon layers, with increasing atomic radius of the subplanted ion. It also suggests the formation of dense phases of the noble gases, simulating solid phases, due to the large forces exerted on the subplanted gases by the graphite layers in their attempt to remain planar.

ACKNOWLEDGMENTS

The authors thank Professor B. M. Pettitt for discussions and guidance concerning the CHARMM model calculations. This material is based on work supported by the National Science Foundation under Grant No. DMR-8914608 and by the Texas Advanced Research Program project No. 3652-211.

[1] D. Marton, in *Low-Energy Ion-Surface Interactions,* edited by J. W. Rabalais (Wiley, New York, in press).
[2] Y. Lifshitz, S. R. Kasi, J. W. Rabalais, and W. Eckstein, Phys. Rev. B **41**, 10 468 (1990).
[3] E. V. Kornelsen, Can. J. Phys. **42**, 364 (1964).
[4] E. V. Kornelson and M. K. Sinha, J. Appl. Phys. **40**, 2888 (1969).
[5] E. V. Kornelsen and M. K. Sinha, J. Appl. Phys. **39**, 4546 (1968).
[6] G. Carter and D. Armour, Thin Solid Films **80**, 13 (1981).
[7] H. J. Steffen, C. D. Roux, D. Marton, and J. W. Rabalais, Phys. Rev. B **44**, 3981 (1991).
[8] H. J. Steffen, D. Marton, and J. W. Rabalais, Phys. Rev. Lett. **68**, 1726 (1992).
[9] D. Marton, K. J. Boyd, T. E. Lytle, and J. W. Rabalais, Surf. Sci. **282**, 113 (1993).
[10] B. R. Brooks, R. E. Bruccoleri, B. D. Olafson, D. J. States, S. Swaminathan, and M. Karples, J. Comput. Chem. **4**, 187 (1983).
[11] L. McDonnell, B. D. Powell, and D. P. Woodruff, Surf. Sci. **40**, 669 (1973).
[12] E. J. Scheibner and L. N. Thorp, Surf. Sci. **8**, 247 (1967).
[13] J. Robertson and E. P. Reilly, Phys. Rev. B **35**, 2946 (1987).
[14] A. Ignatiev, T. N. Rhodin, and S. Y. Tong, Surf. Sci. **42**, 37 (1974).
[15] Polygen Corp., 200 Fifth Ave., Waltham, MA 02254, 1989 Computer Code QUANTA, version 3.2, modified by Molecular Simulations, Inc., Waltham, MA.
[16] A. Bondi, J. Phys. Chem. **68**, 441 (1964).
[17] Z.-M. Chen, O. A. Karim, and B. M. Pettitt, J. Chem. Phys. **89**, 1042 (1988).
[18] J. F. Ziegler, J. P. Biersack, and U. Littmark, *The Stopping*

and Ranges of Ions in Matter (Pergamon, Oxford, 1985), Vol. 1.

[19]W. E. Faust, T. N. O'Neal, and R. L. Chaplin, Phys. Rev. **183**, 609 (1969).

[20]H. Winters, in *Radiation Effects on Solid Surfaces,* edited by M. Kaminsky, *Advances in Chemistry Series* Vol. 158 (ACS, Washington, D.C., 1976), p. 1.

[21]D. J. O'Connor and J. P. Biersack, Nucl. Instrum. Methods Phys. Res. B **15**, 14 (1986).

[22]J. W. Corbett and J. C. Burgoin, in *Point Defects in Solids,* edited by J. H. Crawford, Jr. and L. M. Slifkin (Plenum, New York, 1975), Vol. 2, Chap. 1.

[23]B. T. Kelly, *Physics of Graphite* (Applied Science, London, 1981).

[24]G. L. Montel and G. E. Myers, Carbon **9**, 179 (1971).

[25]H. M. Kramer and J. Suzanne, Surf. Sci. **54**, 659 (1976).